Original Article

Quantitative research on the interaction between cerebral edema and peripheral cerebral blood perfusion using swept-source optical coherence tomography

Jian Liu[1], Yan Li[1], Yang Lin[1], Ziyue Meng[1], Xuyang Guo[2], Yao Yu[1], Zhenhe Ma[1]

[1]School of Control Engineering, Northeastern University at Qinhuangdao, Qinhuangdao, China; [2]Department of Bioengineering, University of Washington, Seattle, USA

Correspondence to: Zhenhe Ma. School of Control Engineering, Northeastern University at Qinhuangdao, Qinhuangdao, China.
Email: mazhenhe@163.com.

Background: Ischemic cerebral edema (CE) is a major leading cause of death in patients with ischemic stroke. The CE progression is closely related to the local cerebral blood perfusion (LCBP) level surrounding the edema area. Quantitative studying the interaction between the CE and peripheral LCBP may provide new inspiration for control and even treatment of CE.

Methods: Photothrombosis ischemia mouse model was established and observed for 9 hours using swept-source optical coherence tomography (SS-OCT). OCT-based angiography and OCT-based attenuation imaging techniques were used to reconstruct the angiograms reflecting the cerebral blood perfusion (CBP) level and optical attenuation coefficient (OAC) maps reflecting the edema state. The influence of edema on LCBP was analyzed by quantifying the blood perfusion in different spatial locations around the edema tissue, and the influence of LCBP on CE progression was revealed by comparing the changes of the edema area and LCBP level over time.

Results: Preliminary studies show that the effect of edema tissue on LCBP is very significant, which shows a clear spatial dependence. LCBP near the edema tissue is 15–20% lower than that far away from the edema tissue. When the LCBP drops to around 60% of the initial value, the edema area increases sharply. In addition, the level of CBP in the contralateral hemisphere also decreases with time. When the contralateral CBP drops to around 60%, there is a certain probability that contralateral edema will occur.

Conclusions: CE progression is not only related to the LCBP around the edema tissue but also related to the CBP of non-edematous regions. Controlling the CBP level of non-edematous regions may play a positive role in the treatment of CE. This work provides a new method and inspiration for exploring the mechanism of ischemic CE progression.

Keywords: Optical coherence tomography (OCT); cerebral edema; local cerebral blood perfusion (LCBP)

Submitted Jul 01, 2020. Accepted for publication Oct 30, 2020.
doi: 10.21037/qims-20-821
View this article at: http://dx.doi.org/10.21037/qims-20-821

Introduction

Ischemic cerebral edema (CE) is a common pathological process that occurs with ischemic cerebrovascular disease. It is the culprit that causes intracranial hypertension and the formation of cerebral hernia. Due to its extremely high mortality and disability rate, CE seriously threatens human physical and mental health (1,2). Quantitative research on the occurrence, development and evolution of ischemic CE can provide a theoretical basis for effective intervention.

Nowadays, many scholars have studied CE from different perspectives and methods, such as water content (BWC) analysis (3), intracranial pressure (ICP) monitoring (4) or

expression of aquaporin (5). Few quantitative analyses have been reported on the interaction between cerebral edema and cerebral blood perfusion (CBP). It is generally accepted that the progression of ischemic CE is closely related to the local cerebral blood perfusion (LCBP) level surrounding the edema area (6). After edema occurs, swelling edema tissue will squeeze the surrounding blood vessels due to the limited intracranial space, causing a decrease in CBP level. When the LCBP surrounding the edema region reduces to a certain level, the edema expands. Such vicious circle is the main factor that threatens the life of patients. Quantitative studies on the relationship between the decline of LCBP and CE progression surrounding edema tissues can help us understand and cope with the vicious cycle.

Optical coherence tomography (OCT) is a real-time, non-invasive and high-resolution imaging modality for three-dimensional (3D) imaging of biological tissues (7). Over the past two decades, OCT has been greatly improved and various OCT-based imaging technologies have been developed. OCT-based angiography (OCTA) (8) and OCT-based attenuation imaging (OCT-AI) (9-11) are two of them, providing 3D blood angiography resolution up to capillary level and attenuation coefficient imaging in tissue beds *in vivo*, respectively. Swept-source OCT (SS-OCT) is a kind of Fourier domain OCT (FD-OCT) with a tunable swept laser as the light source (12-14). Due to its greater light intensity and higher spectral resolution, SS-OCT offers the ability for improved depth and range of imaging (15,16). In our previous work, we have demonstrated the potential of SS-OCT in the simultaneous detection of CBF and CE (17), which paves the way for the study of the progression of brain edema.

In this paper, we present a method for studying the interaction between cerebral edema and peripheral CBP based on SS-OCT. Photothrombosis ischemia mouse model was established and observed for 9 hours. OCTA and OCT-AI techniques were used to reconstruct the angiograms reflecting the CBP state and optical attenuation coefficient (OAC) maps reflecting the edema state. The edema regions were segmented and the LCBP around the edema tissues were quantified. We focused on the relationship between CE progression and LCBP. On the one hand, the influence of edema on LCBP was analyzed by quantifying the blood perfusion in different spatial locations around the edema tissue. On the other hand, the influence of LCBP on CE progression was revealed by comparing the changes of the edema area and LCBP level over time.

Methods

Animal model

Adult male C57BL/6 mice (weight 20–30 g) were used in this study. The study was approved by institutional ethics board of Northeastern University (No. NEU-EC-2020A009S). All efforts were made to minimize animal suffering and to reduce the number of animals used. Surgical anesthesia was induced with sodium pentobarbital (3%, 5 mg/100 g, IP). The anesthetized mice were fixed on a stereotaxic apparatus with ear bars and a clamping device. The fur on the mice's heads was shaved, and the skin was cleaned with saline. The skin was cut along the midline of the skull, and the interparietal bone was exposed by pulling the skin to the sides. Next, the subcutaneous tissue and periosteum were cleaned. Mice were placed under the SS-OCT sample arm for baseline data collection. Then, Rose Bengal (RB, Sigma-Aldrich, St Louis, MO, USA) was injected into the tail vein (20 mg/mL saline, 1 mL/kg bodyweight) and photothrombosis was induced using parallel illumination (532 nm, the diameter of ~2 mm, CNI Laser, MGL-III-532-5mW-1.5, Changchun, China) for 30 minutes. The animal was strictly shielded from light to minimize the diffuse Rose Bengal activation after laser irradiation.

SS-OCT system

A SS-OCT system, established in our previous work (18), was used in this paper. Briefly, the light source employed is a swept-source with a central wavelength of 1,310 nm and a bandwidth of 100 nm. The system operates at a sweep rate of 200 kHz, and the axial resolution in air is ~7.5 μm. Using an objective lens with a focal length of 50 mm allows the system to achieve a lateral resolution of ~16 μm. Although the theoretical ranging depth of the system can reach ~78 mm, in this article we digitized each interference spectrum to 5,000 points, thus providing an actual measurement depth of ~16 mm.

OCTA protocol

OCTA utilizes the intrinsic motion contrast caused by dynamically moving particles (i.e., red blood cells) to distinguish functional blood vessels from static tissue backgrounds. OCTA has been proven to accurately visualize blood vessels including capillaries. Wang *et al.* compared the

vascular images of the mouse brain *in vivo* acquired by both OCT and multiphoton microscopy (MPM) systems (19). They found that OCTA images showed great consistency with the image results obtained from MPM. The blood vessel density in the test area matched well with the MPM results. In our system, the fast scanner (X direction) was driven by a sawtooth waveform with a 160 Hz frame rate, providing a 6.25 ms time interval between adjacent repeated B-scans. Each B-scan image contained 1,000 A-lines that occupied an 80% duty cycle. The slow scanner (Y direction) was driven by a step function waveform, which led to 800 B-scan positions with 4 repeated B-scans per step. The FOV is 8 mm (X direction) ×7.5 mm (Y direction), enough to cover the entire cerebral cortex of mice. First, the initial OCT structure images obtained by the SS-OCT were registered to eliminate motion artifacts. Then, 2D angiograms of each cross-section were obtained by performing first-difference on repeated B-scans, and the 3D angiograms were reconstructed by arranging the 2D angiograms in all cross-section.

OCT-AI protocol

The basic principle of *OCT-AI* is that the power of an incident light beam passes through a biological tissue is attenuated along its path due to scattering and absorption. While, the OAC reflects how quickly the incident light is attenuated and can be used as an indicator of organizational characteristics. Firstly, by averaging the repeated B-scans, we were able to obtain average structural images. The influence of confocal characteristics was removed by dividing by the axial point spread function proposed by van Leeuwen *et al.* (20). Before the OAC calculation, we performed surface extraction and flattened the image. Then, a 3D matrix was reconstructed from the cortex surface, extending a specific number of pixels vertically. An optimized depth-resolved estimation (ODRE) method was used to calculate OAC. In brief, each pixel in OCT dataset was converted to the corresponding OAC value using Eq. [1], under the assumption that backscattered light reflected to the photodetector of the system was a fixed fraction of the attenuated light.

$$\mu[z]=\frac{I[z]}{2\Delta\sum_{i=z+1}^{N}I[i]+\frac{I[N]}{\mu[N]}} \quad [1]$$

where $I[z]$ is the OCT signal of a pixel and $\mu[z]$ is the corresponding OAC, both of which are at depth z. Δ is the pixel size (relative to the axial resolution of the OCT system), and N is pixel numbers within a certain range of depth, $I[N]$ is the OCT signal of the last point N. To determine $\mu[N]$, the data taken from the end of the imaging depth was fitted to an exponential curve with model of $y=a\cdot exp(-2\mu z)+b$. The resulting μ is the average attenuation coefficient of this data and is considered as the best approximation of $\mu[N]$, and b is the strength of the noise floor, which need to be subtracted from the original OCT signal before OAC calculation. After exponential fitting, the fitted μ was introduced into Eq. [1]. A series of *en face* OAC maps were obtained by averaging the OACs in the specific depth range. Last, the edema areas were segmented from the OAC maps. This method is described in detail in our previous article (21).

Quantification of LCBP

In this paper, LCBP is defined as CBP in the local region around the edema tissue, which reflected the blood supply capacity of the local tissue. The quantitative process of LCBP is shown in *Figure 1*. *Figure 1A* is a typical angiogram reconstructed by the OCTA technique. The binary angiogram shown in *Figure 1B* was obtained by dividing the blood vessels on *Figure 1A* using "locally adaptive region growing algorithm" proposed in our previous work (22). *Figure 1C* shows the OAC map reflecting the edema state. The shaded region enclosed by solid red lines is the edema region. We separated this region manually and expanded it using a dilation algorithm, as shown in *Figure 1E*. The local region (*Figure 1F*) was obtained by subtracting the edema area (*Figure 1D*) from the dilated image (*Figure 1E*). Finally, the LCBP map (*Figure 1G*) was obtained by multiplying the local area (*Figure 1F*) with the binary angiogram (*Figure 1B*). It is worth noting that the current LCBP may have errors in reflecting the pathological state of the brain due to various reasons, such as observation location, individual differences or differences in data processing. Therefore, we used the percentage of LCBP at the current stage to that at baseline to represent the level of cerebral perfusion.

Results

A total of 4 mice were used in this study. Before the establishment of the photo phenomenon model, baselines were collected. As shown in *Figure 2*.

After baselines collection, mice were injected with Rose Bengal and irradiated with a 532 nm laser for 30 minutes,

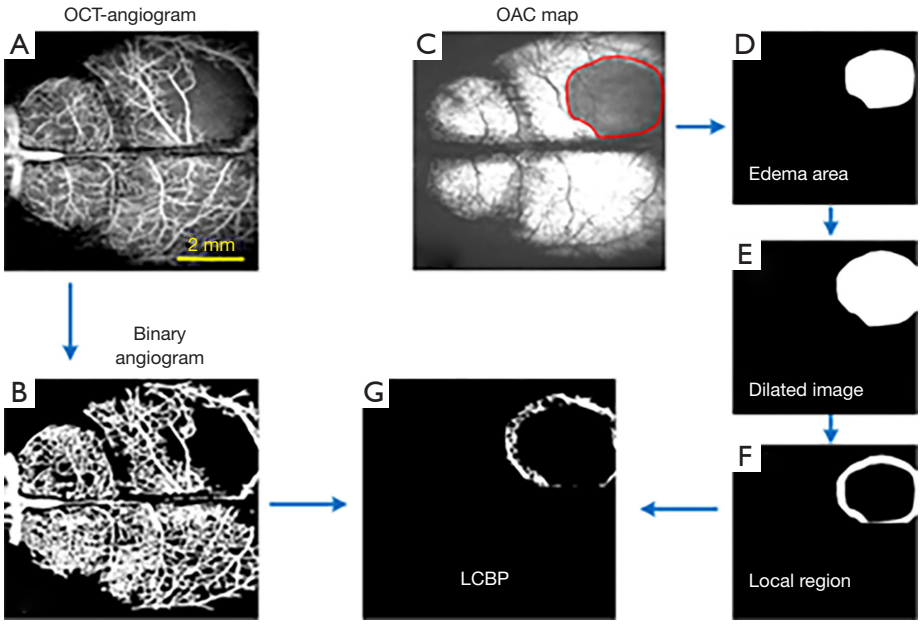

Figure 1 Quantitative process of LCBP. (A) A typical OCT angiogram obtained by SS-OCT. (B) The corresponding binary angiogram. (C) The corresponding OAC map, the shaded region enclosed by solid red lines is the edema region. (D) Edema area. (E) The Dilated image of (D). (F) The local region obtained by subtracting edema area (D) from dilated image (E). (G) The LCBP map obtained by multiplying the local area (F) with the binary angiogram (B). LCBP, local cerebral blood perfusion; SS-OCT, swept-source optical coherence tomography; OAC, optical attenuation coefficient.

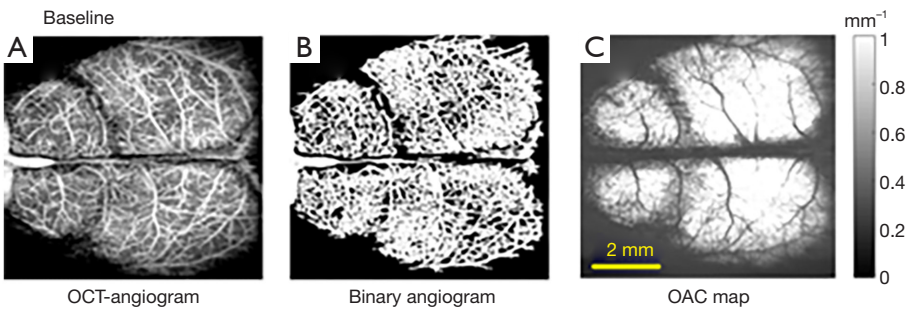

Figure 2 Baseline of OCT-angiogram, binary angiogram and OAC map of the entire parietal cortex in mice. OCT, optical coherence tomography; OAC, optical attenuation coefficient.

and then were observed for 9 hours using SS-OCT. As shown in *Figures 3*,*4*.

The first column in *Figure 3* was collected immediately after modeling, named 0 h in the timeline. Data were collected every half an hour within 2 hours, and every 1 hour after 2 hours, and up to 9 hours. *Figure 3* shows the progress of CBP and CE from 0 to 3 h. It was shown that CBP gradually decreases with time, and the vascular loss in the infarction area becomes more and more serious. As can be seen from the edema maps that although the OAC value decreased gradually with time (the decrease of OAC value meant the increase of water content in brain tissue), the range of edema changed slowly, while the LCBP around the edematous tissue had gradually decreased due to extrusion. After 3 hours, the edema area began to increase rapidly, as shown in *Figure 4*.

Figure 4 shows the changes of CBP and CE from 4 to 9 h. As can be seen from *Figure 4* that the edema area is getting larger and larger, and the region with low or no perfusion is also getting larger and larger. Based on binary angiograms

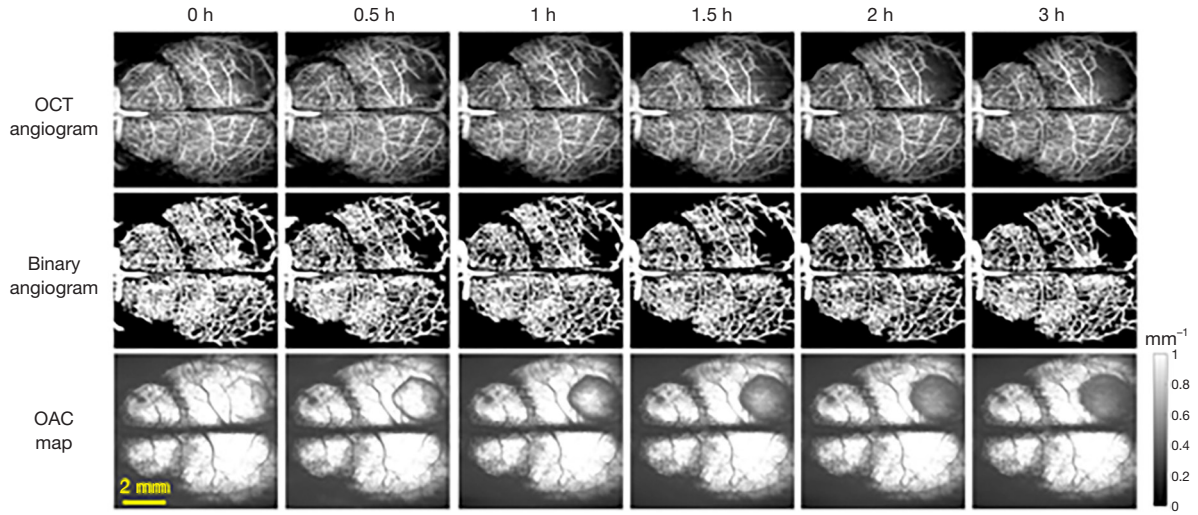

Figure 3 The progression of CBP and CE with time from 0 to 3 h. CBP, cerebral blood perfusion; CE, cerebral edema.

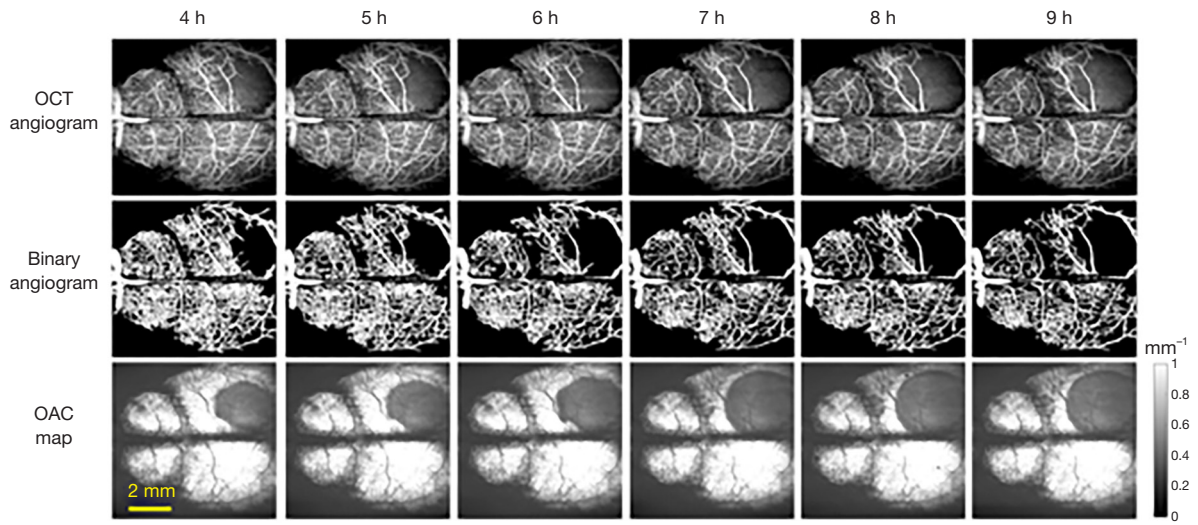

Figure 4 The change of CBP and CE with time at 4~9 h. CBP, cerebral blood perfusion; CE, cerebral edema.

and OAC maps obtained by SS-OCT, the relationship between the CBP and CE progression was studied from two perspectives. First: the effect of edema on LCBP. As shown in *Figure 5A*, we manually marked the boundary of the edema tissue on the OAC maps at each time point, and then extended the boundary outwards using the "dilation" algorithm, each time expansion is 80 microns (10 pixels), a total of 10 expansions. So far, 10 circular regions have been formed around the edema of each OAC image. LCBP levels in 10 regions at 1, 3, 6 and 9 h were analyzed (n=4). Sagittal sinus veins were not included in the statistical range due to their inconspicuous changes.

Before 3 hours, as shown in *Figure 5B,C*, LCBP shows a clear spatial dependence. LCBP near the edema tissue is 15–20% lower than that far away from the edema tissue. A variety of factors, including blood flow occlusion and edema-occupying effects, have contributed to the decrease in LCBP. After 3 hours, LCBP in areas far from the edema border also showed a low level. This is because prolonged ischemia leads to a decrease in the level of global cerebral blood perfusion.

Second: the effect of LCBP on edema. Local areas in the

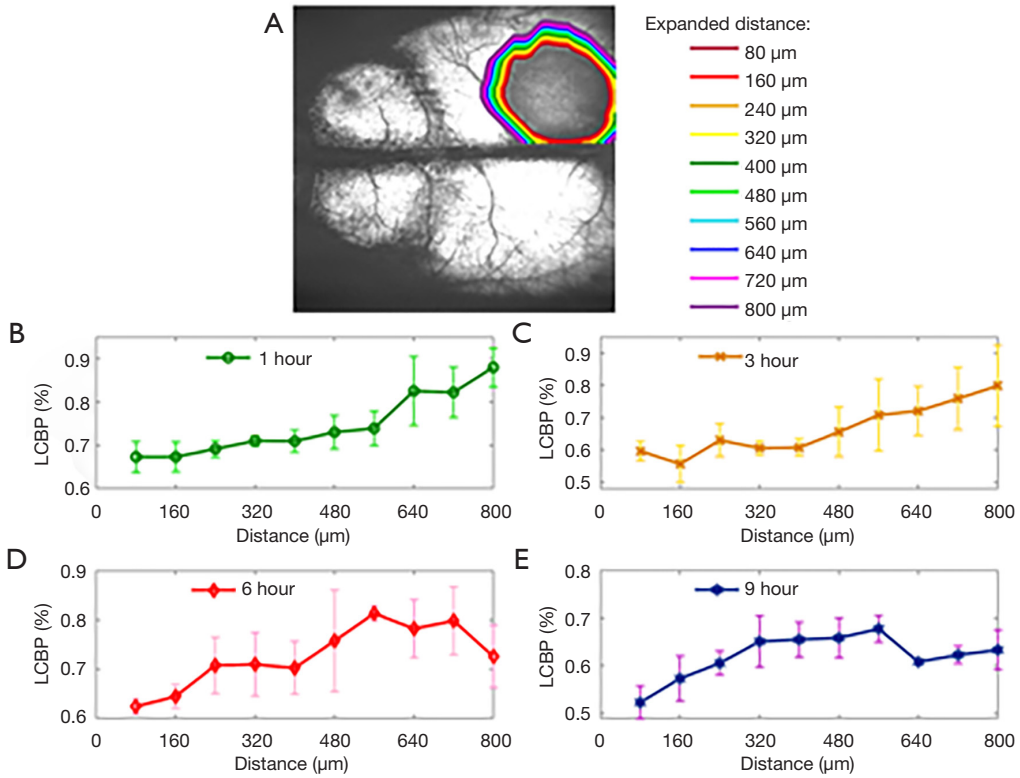

Figure 5 The effect of edema on LCBP. (A) 10 local areas around the edema tissue. (B-E) LCBP levels in 10 regions at 1, 3, 6 and 9 h, respectively. Data were presented as mean ± SD (n=4). LCBP, local cerebral blood perfusion.

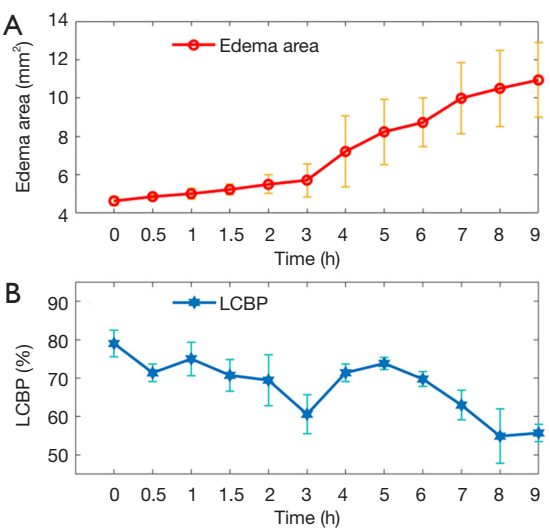

Figure 6 The edema area over time (A) and the percentage of LCBP over time (B). Data were presented as mean ± SD (n=4). The local areas are in 400-micron range (50 pixels) beyond the edema boundary. LCBP, local cerebral blood perfusion.

400 micron range (50 pixels) beyond the edema boundary were selected for analysis. The LCBP and edema area curve over time is shown in *Figure 6*. *Figure 6A* shows the edema area over time (n=4) and *Figure 6B* shows the percentage of LCBP over time (n=4).

We found that during 0–3 h, the area of edema tissue expanded slowly, and LCBP fluctuated slightly around 70% with a slight overall decline. At 3 h, LCBP dropped down to 60%±5%, and the CE area increased more rapidly thereafter. We also found that LCBP rebounded and returned to around 70% after 4 hours. The main reason is that the LCBP region quantified by us is a local region outside the edema boundary. When the edema area expands, the location of the local region also changes and the LCBP in this region is still at a relatively normal level at this time. After 8 h, LCBP gradually decreased again to around 60%. Besides, we also found that the level of CBP outside the edema region also decreased with time. *Figure* 7 shows the CBP changes in areas outside the maximum edema range.

A study has shown that when the brain on one side has

prolonged ischemia, the other half of the brain may also develop edema (23). This phenomenon may be caused by the CBP level in non-edematous regions falling to a critical value (i.e., the threshold). In this study, one of the four mice developed contralateral edema, as indicated by the red arrow in *Figure 8*.

Discussion

Cerebral edema is one of the main complications of ischemic stroke. When cerebral ischemia occurs, ATP decreased and the sodium pump on the cell membrane starts to fail, unable to discharge the excess sodium ions from the cell. Chloride ions enter the cell and combine with sodium ions to form sodium chloride, thereby increasing the intracellular osmotic pressure. A large amount of water enters the cell from the outside to maintain the balance of osmotic pressure inside and outside the cell. At this moment, cerebral edema has formed. Edema in this state is called cytotoxic edema. It is characterized by cell swelling in the brain tissue, but the blood brain barrier (BBB) remains intact. As ischemia progresses, capillary permeability increases and the BBB is destroyed. The plasma proteins, water, and electrolytes in the capillaries overflow outside the blood vessels, and the water accumulates in the extracellular space, forming vasogenic cerebral edema (24). Therefore, ischemia is the main cause of edema.

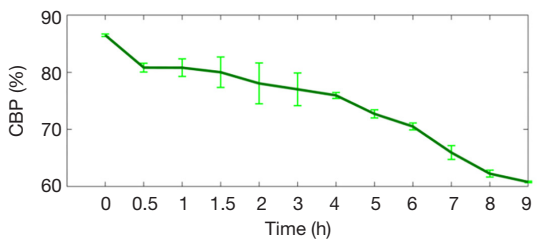

Figure 7 Changes of CBP in areas outside the maximum edema range over time. CBP, cerebral blood perfusion.

The reason why malignant cerebral edema has become the most important lethal factor in ischemic stroke is that the vicious circle between edema and ischemia. To explore the vicious circulation mechanism of ischemic CE progression, answers to two questions are required: first, how does the edema tissue affect the peripheral LCBP? Second, how does peripheral LCBP in turn affect the progression of edema? To solve these problems, a suitable animal model is needed to reveal the mechanism of CE progression, and a powerful imaging device is also necessary which can simultaneously monitor the physiological states of CBP and CE for research.

The photothrombosis ischemia model, first established by Watson *et al.* (6,25) in 1985, can meet the requirements of this study. The basic principle is that after injecting a certain amount of circulating photosensitive dye into an animal and irradiating it with a specific light wave at a certain spot, the photochemical reaction causes to focal disruption of the endothelium at the particular site, which activates platelets, lead to the fibrin clot deposition, and eventually results in occlusion of the microvasculature. The thrombosis process in this model is similar to that in the human brain, with a small injury, without skull damage and has good repeatability. Unlike other models of stroke, photothrombosis permits a tightly regulated location and size of infarct. These characteristics mean that this model is suitable for studying the mechanism of ischemic CE progression.

On the other hand, an ideal technique for evaluating the CE progression mechanism in small animals should have the capillary resolution for angiography and sufficient sensitivity for edema imaging. In order for long-term characterization, it is imperative that the system is non-invasive and does not require any exogenous contrast agents. Besides, CBP and

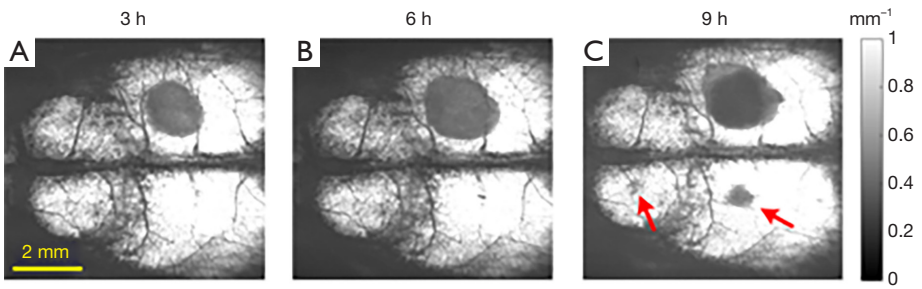

Figure 8 Edema appeared on the healthy side of the brain. The red arrows point out the location of the edema.

CE should be detected simultaneously. Otherwise, there will be a time difference between the two, affecting the accuracy of the assessment. In this paper, the relationship between LCBP and edema progression was analyzed with 9 h monitor of the photothrombotic ischemia mouse model using SS-OCT.

According to *Figure 6* we found that from 0 to 3 h, the edema area increased slowly, and LCBP was around 70% and decreased slowly. At 3 h, LCBP decreased to 60%±5%, after which there was a sharp increase in the area of edema. Therefore, we speculate that 60%±5% may be a dangerous threshold and it may trigger a new round of edema if LCBP approaches this level. In clinical treatment, appropriate interventions may need to be performed before LCBP falls to this critical value.

According to *Figure 5*, the closer the area to the edema tissue, the lower the LCBP is, and vice versa, with a difference of 15–20%. It can be considered that if the LCBP can be controlled at a level above 60%±5%, then the CBP of the non-edematous regions must be at least 80%. We also note that the CBP in non-edematous regions at 2 h is about 78% (*Figure 7*), which is less than 80%. Immediately, LCBP decreased at 3 h. Perhaps one of the conditions to avoid the malignant progression of CE is to ensure that the CBP in the non-edema regions is controlled at ~80% of the initial level. Obviously, the progression mechanism of cerebral edema is much more complicated. There are many factors that contribute to CE, such as blood-brain barrier destruction and leukocyte infiltration. It is also necessary to perform many experiments to determine how much the CBP is involved.

In *Figure 7*, the CBP in the non-edematous region was below 65% at 9 hours, and is approaching the threshold for inducing edema. In our results, only one of the four mice developed contralateral edema. Other mice did not show similar effects, probably due to individual differences or because the observation time was not long enough. Therefore, the study on the CBP level and CE progression mechanism is very important for both treatment of the edema region and the prevention of non-edematous regions.

In conclusion, exploring the mechanism of ischemic CE progression is of great significance for the selection of treatment strategies. Preliminary studies showed that CE progression is not only related to the LCBP around the edema tissue but also related to the CBP of non-edematous regions. Controlling the CBP level of non-edematous regions may play a positive role in the treatment of CE. This work provides a new method and inspiration for exploring the mechanism of ischemic CE progression.

Acknowledgments

Funding: This work was supported in part by National Natural Science Foundation of China (61771119 and 61901100), Hebei Provincial Natural Science Foundation of China (H2018501087 and H2019501010). Fundamental Research Funds for the Central Universities (N182304008).

Footnote

Provenance and Peer Review: With the arrangement by the Guest Editors and the editorial office, this article has been reviewed by external peers.

Conflicts of Interest: All authors have completed the ICMJE uniform disclosure form (available at http://dx.doi.org/10.21037/qims-20-821). The special issue "Advanced Optical Imaging in Biomedicine" was commissioned by the editorial office without any funding or sponsorship. The authors have no other conflicts of interest to declare.

Ethical Statement: The study was approved by institutional ethics board of Northeastern University (No. NEU-EC-2020A009S).

References

1. Faul M, Wald MM, Xu L, Coronado VG. Traumatic Brain Injury in the United States: Emergency Department Visits, Hospitalizations and Deaths 2002-2006. 2010.
2. Ayata C, Ropper AH. Ischaemic brain oedema. J Clin Neurosci 2002;9:113-24.
3. Slivka A, Murphy E, Horrocks L. Cerebral edema after temporary and permanent middle cerebral artery occlusion in the rat. Stroke 1995;26:1061-5; discussion 1065-6.

4. Koenig MA. Cerebral Edema and Elevated Intracranial Pressure. Continuum (Minneap Minn) 2018;24:1588-602.
5. Zador Z, Stiver S, Wang V, Manley GT. Role of aquaporin-4 in cerebral edema and stroke. In: Aquaporins. Berlin, Heidelberg: Springer, 2009:159-70.
6. Manwaring PK, Moodie KL, Hartov A, Manwaring KH, Halter RJ. Intracranial electrical impedance tomography: a method of continuous monitoring in an animal model of head trauma. Anesth Analg 2013;117:866-75.
7. Wang RK. Optical Microangiography: A Label Free 3D Imaging Technology to Visualize and Quantify Blood Circulations within Tissue Beds in vivo. IEEE J Sel Top Quantum Electron 2010;16:545-54.
8. Chen CL, Wang RK. Optical coherence tomography based angiography [Invited]. Biomed Opt Express 2017;8:1056-82.
9. Faber D, van der Meer F, Aalders M, van Leeuwen T. Quantitative measurement of attenuation coefficients of weakly scattering media using optical coherence tomography. Opt Express 2004;12:4353-65.
10. Vermeer KA, Mo J, Weda JJ, Lemij HG, de Boer JF. Depth-resolved model-based reconstruction of attenuation coefficients in optical coherence tomography. Biomed Opt Express 2013;5:322-37.
11. Smith GT, Dwork N, O'Connor D, Sikora U, Lurie KL, Pauly JM, Ellerbee AK. Automated, Depth-Resolved Estimation of the Attenuation Coefficient From Optical Coherence Tomography Data. IEEE Trans Med Imaging 2015;34:2592-602.
12. Yun S, Tearney G, Bouma B, Park B, de Boer J. High-speed spectral-domain optical coherence tomography at 1.3 mum wavelength. Opt Express 2003;11:3598-604.
13. Song S, Xu J, Wang RK. Long-range and wide field of view optical coherence tomography for in vivo 3D imaging of large volume object based on akinetic programmable swept source. Biomed Opt Express 2016;7:4734-48.
14. Xu J, Song S, Wei W, Wang RK. Wide field and highly sensitive angiography based on optical coherence tomography with akinetic swept source. Biomed Opt Express 2016;8:420-35.
15. Adhi M, Liu JJ, Qavi AH, Grulkowski I, Lu CD, Mohler KJ, Ferrara D, Kraus MF, Baumal CR, Witkin AJ, Waheed NK, Hornegger J, Fujimoto JG, Duker JS. Choroidal analysis in healthy eyes using swept-source optical coherence tomography compared to spectral domain optical coherence tomography. Am J Ophthalmol 2014;157:1272-81.e1.
16. Spaide RF, Koizumi H, Pozzoni MC. Enhanced depth imaging spectral-domain optical coherence tomography. Am J Ophthalmol 2008;146:496-500.
17. Liu J, Li Y, Yu Y, Yuan X, Lv H, Liu L, Zhao Y, Wang Y, Ma Z. Simultaneous detection of cerebral blood perfusion and cerebral edema using swept-source optical coherence tomography. J Biophotonics 2020;13:e201960087.
18. Liu J, Ding N, Yu Y, Liu L, Yuan X, Lv H, Zhao Y, Ma Z. Whole-brain microcirculation detection after ischemic stroke based on swept-source optical coherence tomography. J Biophotonics 2019;12:e201900122.
19. Wang H, Baran U, Li Y, Qin W, Wang W, Zeng H, Wang RK. Does optical microangiography provide accurate imaging of capillary vessels?: validation using multiphoton microscopy. J Biomed Opt 2014;19:106011.
20. van Leeuwen TG, Faber DJ, Aalders MC. Measurement of the axial point spread function in scattering media using single-mode fiber-based optical coherence tomography. IEEE J Sel Top Quantum Electron 2003;9:227-33.
21. Liu J, Ding N, Yu Y, Yuan X, Luo S, Luan J, Zhao Y, Wang Y, Ma Z. Optimized depth-resolved estimation to measure optical attenuation coefficients from optical coherence tomography and its application in cerebral damage determination. J Biomed Opt 2019;24:1-11.
22. Ma Z, Ding N, Yu Y, Ma Y, Yuan X, Wang Y, Zhao Y, Luan J, Liu J. Quantification of cerebral vascular perfusion density via optical coherence tomography based on locally adaptive regional growth. Appl Opt 2018;57:10117-24.
23. Toung TJ, Hurn PD, Traystman RJ, Bhardwaj A. Global brain water increases after experimental focal cerebral ischemia: effect of hypertonic saline. Crit Care Med 2002;30:644-9.
24. Hatashita S, Hoff JT. Role of blood-brain barrier permeability in focal ischemic brain edema. Adv Neurol 1990;52:327-33.
25. Watson BD, Dietrich WD, Busto R, Wachtel MS, Ginsberg MD. Induction of reproducible brain infarction by photochemically initiated thrombosis. Ann Neurol 1985;17:497-504.

Cite this article as: Liu J, Li Y, Lin Y, Meng Z, Guo X, Yu Y, Ma Z. Quantitative research on the interaction between cerebral edema and peripheral cerebral blood perfusion using swept-source optical coherence tomography. Quant Imaging Med Surg 2021;11(3):939-947. doi: 10.21037/qims-20-821

